105 GHz Notch Filter Design for Collective Thomson Scattering

Furtula, Vedran; Michelsen, Poul; Leipold, Frank; Johansen, T.; Korsholm, Søren Bang; Meo, Fernando; Moseev, Dmitry; Nielsen, Stefan Kragh; Salewski, Mirko; Stejner Pedersen, Morten

Published in:
Fusion Science and Technology

Publication date:
2011

105 GHz Notch Filter Design for Collective Thomson Scattering

V. Furtula, P. K. Michelsen, F. Leipold, M. Salewski,
S. B. Korsholm, F. Meo, D. Moseev, S. K. Nielsen, and M. Stejner
Association Euratom - Risø National Laboratory for Sustainable Energy,
Technical University of Denmark, DK-4000 Roskilde, Denmark

T. Johansen
DTU Elektro, Technical University of Denmark, DK-2800 Lyngby, Denmark

(Dated: September 3, 2010)

Abstract

A mm-wave notch filter with 105 GHz center frequency, more than 20 GHz passband coverage, and 1 GHz rejection bandwidth has been constructed. The design is based on a fundamental rectangular waveguide with cylindrical cavities coupled by narrow iris gaps, i.e. small elongated holes of negligible thickness. We use numerical simulations to study the sensitivity of the notch filter performance to changes in geometry and in material conductivity within a bandwidth of $\pm$ 10 GHz. The constructed filter is tested successfully using a vector network analyzer monitoring a total bandwidth of 20 GHz. The typical insertion loss in the passband is below 1.5 dB, and the attenuation in the stopband is approximately 40 dB.

I. INTRODUCTION

In magnetic confinement devices, such as tokamaks or stellarators, mm-wave notch filters are used to protect diagnostic instruments from gyrotron stray radiation. Typical mm-wave diagnostics are electron cyclotron emission (ECE) spectroscopy, reflectometry, and collective Thomson scattering (CTS) [1]. Gyrotrons produce high power mm-waves and are used for electron cyclotron resonance heating (ECRH) and current drive (ECCD) [2, 3], for mitigation of tearing modes [4], and as a probing radiation source in CTS experiments [5–7]. Notch filters can make mm-wave plasma diagnostics compatible to plasma experiments with gyrotron operation.

The tokamak ASDEX Upgrade is equipped with dual frequency 1 MW gyrotrons [2, 3]. Operation at 140 GHz is used for ECRH and ECCD [2, 3]; operation at 105 GHz is used for CTS experiments [5–7]. The velocity distribution function of fast ions [7–10] and the ion temperature [11] have been measured on various magnetic confinement devices using CTS. Important prerequisites for CTS measurement of the fuel ion ratio have been demonstrated [12, 13], and it may also be possible to infer the ion rotation and the ion densities [14].

The requirement for the notch filter rejection bandwidth depends on whether stray radiation from a single gyrotron or from many gyrotrons has to be blocked. For a single gyrotron, a rejection bandwidth of 130 to 200 MHz centered at the nominal gyrotron frequency is sufficient to accommodate gyrotron chirp [5]. CTS experiments require only a single gyrotron. The front-end CTS receiver has two notch filters in series which strongly attenuate the gyrotron stray radiation. The rejection bandwidth has to be as narrow as possible since otherwise valuable information about the distribution of bulk ions would be lost. Depending on scattering geometry and bulk ion temperature, the width of the measured bulk ion CTS spectra can be as narrow as ± a few hundred MHz. The CTS passband required for the notch filter is ± 5 GHz wide (ASDEX Upgrade), so as to measure fast deuterons with energies up to 500 keV [5].

If many gyrotrons are used, typical for ECRH or ECCD, the notch filter rejection bandwidth has to be wider due to slightly different center frequencies of the gyrotrons (from 500 MHz to 1 GHz [5, 15]). A notch filter with a relatively broad stopband has recently been presented [15]. The ECE spectroscopy system at ASDEX Upgrade requires a notch

filter with rejection depth of 60 dB and notch bandwidth of ∼1 GHz since several gyrotrons are used simultaneously [3]. Additionally, these notch filters should have a broad passband to cover the ECE band, they should have a low, frequency independent insertion loss, and the portion of reflected power should be low. The ECE spectroscopy system at ASDEX Upgrade requires a passband of ±9 GHz in order to cover the complete plasma ECE range [3].

Diagnostics using mm-waves can well be used in the strongly radiative environment of future plasma confinement devices with fusion processes [16], and gyrotrons are also foreseen for such devices. Several gyrotrons are foreseen to be installed on ITER with frequencies of 170 GHz for ECRH and ECCD [17, 18], of 120 GHz for machine start-up [19, 20] and of 60 GHz for the CTS diagnostic [21–24]. ITER will most probably be equipped with reflectometry diagnostic [25, 26] and ECE spectrometry [27, 28]. So notch filters will be necessary for ITER. Several options of notch filters for ITER are available [29]. F-band notch filters with notch frequencies up to 140 GHz and up to 100 dB rejection and passband coverage of several GHz have been designed [15, 30–34]. Waveguide notch filters with a center frequency below 100 GHz have also been presented [35]. Notch filters for higher frequencies are more difficult to construct as the dimensions of the filter become so small that machining becomes difficult [29]. However, one can use quasi-optical resonance notch filters [36–38] or the absorption lines of molecules [29, 39].

This paper will present the design of a compact and sensitive F-band notch filter with 1 GHz rejection bandwidth and a possibility of tuning the center frequency ±2%. We measure the spectral response of the notch filter and compare it with numerical simulation. Additionally, we assess the sensitivity to changes in physical parameters and in material conductivity by S-parameter simulation.

II. IRIS COUPLED T-JUNCTION IN A CIRCULAR WAVEGUIDE

If a waveguide with uniform cross-section is terminated at both ends by metal planes perpendicular to the axis of the guide and if the guide length is equal to a full number of half wavelengths, $\lambda_g/2$ where λ_g is defined as the distance between two equal phase planes along the waveguide, electromagnetic fields can resonate in the guide. Such a waveguide can be a cylindrical cavity and is used here to form a tunable notch filter. Requirements for the notch filter are: relatively narrow 3 dB rejection bandwidth ($\frac{BW_{3dB}}{f_0} \ll 1$), center frequency

f_0∼105 GHz, and passband of at least 18 GHz centered at f_0. The 3 dB rejection bandwidth BW_{3dB} is defined here as a bandwidth between the two 3 dB points of the insertion loss. A way to design such a notch filter [40] is to use a symmetrical right-angle T-type junction of a rectangular and a circular guide coupled by a small elliptical aperture (iris) in a metallic wall of negligible thickness as shown in fig. 1. A great benefit of an iris design is the simple cavity adjustment with only a single tuning screw per cavity. The major axis of the elliptical aperture forms the angle ϕ with respect to the vertical axis. The angle ϕ is restricted to 0° to ensure good coupling to all the TE_{nml} modes and among these the fundamental TE_{111} mode in a cylindrical cavity. The subscript n refers to the number of circumferential (ϕ) variations, m refers to the number of radial (ρ) variations, and l refers to the full number of half wavelengths along the z axis according to the cylindrical coordinate system (ρ, ϕ, z). The fundamental mode has optimum passband coverage and relatively low loss compared with higher order modes. If we choose ϕ=90°, transverse magnetic (TM) modes will be dominant inside the resonant cavity.

In the main guide the TE_{10} mode exists and is the fundamental mode for the rectangular waveguide. From the previous discussion we know that an iris wall has no thickness, but we choose an aperture in the metallic wall with 0.2 mm thickness because smaller sizes cannot be realized. The finite iris thickness introduces only a slight translation in frequency characteristics. The effect is small because 0.2 mm is much smaller than the vacuum wavelength λ_0=c/f_0=2.86 mm. The cut-off wavelength λ_c determines the lowest frequency in a waveguide. For the main guide λ_c=2a=4.06 mm, where a=2.03 mm is the broad side of the guide. A waveguide with circular cross-section has a cut-off wavelength $\lambda_{c,nm}$=$\pi D/p'_{nm}$ where D=2 mm is the cavity diameter and p'_{nm} is the m'th root of the derivative of first order Bessel function $J'_n(p'_{nm})$=0. For the TE_{11l} mode we find the cut-off wavelength $\lambda_{c,11}$=2π/1.841=3.41 mm, i.e. $\lambda_c > \lambda_0$ as required. The desirable distance between two resonators is an odd number of quarter wavelengths, so the notches can be tuned independently of each other:

$$\Delta l = \frac{\lambda_g}{4}\,(1+2N) \quad \text{where} \quad \lambda_g = \frac{\lambda_0}{\sqrt{1-\left(\frac{\lambda_0}{\lambda_c}\right)^2}}, \tag{1}$$

and N=$\{0, 1, 2\ldots\}$. The wavelength for the main guide is λ_g=4.0 mm and ideally N=0; we get Δl=1.0 mm. Setting N=0 will give us minimum insertion loss but the Δl value

will leave no space for the tuning screw thread. The simulations have shown that a slightly higher value for Δl (Δl=1.3 mm) will have a negligible impact on the notch shape since the resonance frequencies are not affected by the distance Δl but only by the cavity length d and by the diameter D. The constructed notch filter and the 3-D graphical sketch are shown in fig. 2.

Figure 3 shows the four fundamental transverse electric (TE) modes appearing in a cylindrical cavity resonator: TE_{11l}, TE_{21l}, TE_{01l}, and TE_{31l}. Each mode is plotted with the first three resonating lengths $d=l\lambda_g/2$ where $l=\{1,2,3\}$. Using eq. 1 and assuming cavity modes TE_{11l} with λ_c=3.41 mm we find that λ_g=5.2 mm where possible resonator lengths are $d=\{2.6, 5.2, 7.8\ldots\}$ mm. The distance between the curves along the vertical direction shows the distribution of resonance frequencies when D/d is constant. The product of resonance frequency and cavity diameter of our notch filter is f_rD=21 [GHz-cm] resulting in $D/d\sim$0.77 for the TE_{111} mode. The calculated cavity length becomes d=2.6 mm. The chosen point of resonance can vary $\pm$10 GHz without intercepting another resonance line which means there are no other notches within this band. This is the main reason why we operate the notch filter using the fundamental TE_{111} mode.

III. EXPERIMENTAL AND NUMERICAL METHODS

The notch filter is measured using a broadband Anritsu millimeter wave vector network analyzer (VNA) ME7808B with a calibrated bandwidth of 20 GHz. A pair of waveguide tapers has been used to adapt the WR-8 notch filter ports to the WR-10 VNA ports. The port 1 test power is approximately +2 dBm, and the output dynamic range is approximately 60 dB (for a sweep of 2 s) which is sufficient for us to localize the notches.

In the simulations we solve Maxwell's equations and boundary conditions which describe the electromagnetic field distribution inside a waveguide and resonator cavities. If we know the fields existing in the structure, we can uniquely determine the scattering parameters. CST Microwave Studio with a real time domain simulator based on the finite element method is used to characterize the filters. For the simulation we assume air as medium where the fields can exist; the notch filter body is chosen to be copper. The notch filter is excited using waveguide ports at the ends of the main rectangular guide.

IV. MEASURED AND COMPUTED NOTCH FILTER PERFORMANCE

The center frequencies of the measured and the simulated notch filters, shown in figure 4, coincide as expected. The measured notch filter has a much wider 3 dB rejection bandwidth, approximately 1.8 GHz, compared with the simulated value of approximately 380 MHz. The quality factor, or Q factor, with $Q \sim \frac{f_0}{BW_{3dB}}$ is then lower for the constructed filter by a factor 5 compared with the simulated filter. It is known that instabilities in the mechanics such as loose tuning screws or tuning plates, low torque on assembly screws, etc., can have negative impact on the Q factor due to cross coupling or leakage.

Fig. 5 (left) shows the spectral position of the modes in a 45 GHz bandwidth range. The cutoff frequency is located around 73 GHz due to the rectangular waveguide dimensions (WR-8). Below the cut-off no wave can propagate through the filter. The frequency resolution in fig. 5 (left) is not sufficient to resolve the spectral region centered about the notch at 105 GHz, and the notch depth cannot be obtained with this coarse resolution. We increase the frequency resolution in fig. 5 (right) by a factor of 5 where the frequency step is much smaller than the 3 dB bandwidth. In addition $\lambda_{mesh} \ll \lambda_g$ is hard to keep when simulating strongly resonating structures (such as a filter) due to relatively long solving time. The measurements have demonstrated that the notch depth is strongly dependent on the attachment between the tuning screws and the filter body and can vary up to ± 10 dB when shifting the center frequency by ± 2 %. The filter Q factor can be degraded, so mechanical stability of the tuning screws will increase the notch depth with less variation during adjustment.

V. SENSITIVITY STUDY OF THE COMPUTED RESULTS

In this section we address the sensitivity of the computed results to changes in physical and numerical parameters. We consider first how the results change when the mesh is refined. Second, we consider how the results depend on the key geometry parameters. The sensitivity to all parameters, physical and numerical, has a bearing on the accuracy of the comparison between the computed and measured results. Figure 6 shows the notch frequency, the 3 dB bandwidth, and the shape factor, BW_{20dB}/BW_{3dB}, as a function of lines per wavelength where $L/\lambda_0 = 20$ corresponds to 1.4 million meshcells. The shape factor measures how efficient the filter is in the rejection band. For instance if the 3 dB rejection bandwidth is 1 GHz and

the shape factor is 0.8, then we can be sure that a bandwidth of 800 MHz will reject at least 20 dB of the input signal centered around f_0. The center frequency changes by few tens of MHz if increasingly finer meshes are used, the 3dB bandwidth settles in the range from 340 to 370 MHz and the shape factor from 0.51 to 0.55. These ranges show how accurate the parameters could be determined by the simulation, given the physical parameters were set correctly. But the results are highly sensitive to the physical parameters, and so the grid accuracy gives only an incomplete picture. We will now demonstrate the sensitivity of the results to physical or geometrical parameters: the cavity length, the iris width, the iris length, and lastly the material choice.

The new design for the F-band notch filter is found to differ from a previous design [15]. The center frequency is nearly eight times more sensitive to change in the cavity length with the gradient of -11.32 GHz/mm as seen in the upper graph in fig. 7. Higher sensitivity enhances the possibility to move the resonance frequencies up or down making the notch filter more attractive for other experiments. The 3 dB rejection bandwidth is less sensitive compared with the design in [15], and has a slope of -50 MHz/mm. The shape factor has values in the range from 0.51 to 0.53, which are acceptable. The sensitivity analysis results are reported in table II.

The six cavities have the same length in the simulations. The initial cavity lengths d typed in the simulator environment are calculated by hand using theory described in section II. The length between two cavities, Δl, is calculated from the theory in section II and is not optimized in the simulator. Any resonances that appear in the range 90 to 140 GHz are due to cylindrical cavities only. The filter coupling geometry can help us to excite certain modes better than others, but shifting in frequency or creating and destroying modes is not possible by changing coupling geometry.

The iris width (see fig. 1) has relatively small impact on the slope of the center frequency but high impact on the 3 dB bandwidth as seen from fig. 8. The shape factor gets even better with the iris width but at the same time the 3 dB bandwidth gets larger. The key values for the iris width are reported in table II.

The iris length is interesting since it shows non-linear dependence of the 3 dB bandwidth as shown in fig. 9. The iris length must be kept at approximately 1.9 mm in order to keep the rejection bandwidth narrow. For this iris length, the sensitivity of the 3 dB rejection bandwidth with respect to changes of the iris length is small as can be seen from the curve

gradient. Small imperfections in the machining have a small effect on the rejection width. For the calculated points that are well distributed along a straight line the least squares method is used to determine the slope.

If we choose to set the iris width to 0.2 mm, the 3 dB rejection bandwidth will, according to the simulations, get 162 MHz broader. The 3 dB rejection bandwidth is less sensitive to the iris width (3.98 GHz/mm) compared with the iris length (-6.13 GHz/mm) as shown in table II. The iris length should not be short compared with the cavity diameter, since otherwise the 3 dB rejection bandwidth will increase. The lowest rejection bandwidth is achieved if the iris length is comparable to the cavity diameter.

The material choice is an important factor when trying to minimize conductor loss. The insertion loss curve shifts down in level when the conductor loss increases causing broader 3 dB rejection bandwidth, which is not what we aim for. A clear difference of few dBs among conductors appears at the passband shoulders as seen in fig. 10. The lower graphs in fig. 10 have opposite slopes where the 3 dB bandwidth decreases while the shape factor increases with conductivity of the filter body. This implies that the quality factor Q of the resonators improves as expected from theory. This phenomenon is not observed for geometrical parameters such as cavity length and iris width and length, meaning that there is always a trade-off among geometrical parameters in order to achieve the optimum filter characteristics.

Commonly either copper (σ=$5.96 \cdot 10^7$ S/m) or silver-coating (σ=$6.3 \cdot 10^7$ S/m) are used as material for frequencies above 110 GHz. We use copper for construction of the filter body and brass for the tuning screws. Brass is a harder metal than copper and thereby useful for the mechanical parts that can wear out quickly, such as tuning screws.

VI. DISCUSSION AND CONCLUSIONS

A notch filter using T-junction iris coupling (fig. 1), 20 GHz passband coverage, and 1.8 GHz rejection bandwidth has been presented fulfilling the design requirements mentioned in the beginning of section II. The key filter parameters such as center frequency f_0, 3 dB rejection bandwidth BW_{3dB}, and shape factor were investigated by adjusting the filter geometry slightly. The center frequency of the filter is found to be sensitive to the cavity length, which is beneficial for the dynamic notch shifting across the spectrum.

The filter parameters are sensitive to small inaccuracies in the milling process or to cavity tuning. From the simulation data compiled in table II we see that the filter geometry have impact on the filter parameters. How crucial these influences are depends on the filter requirements. A notch filter design should have a low sensitivity to geometrical changes in its center frequency, 3 dB bandwidth, and shape factor. It is clear from the simulations that the iris width is the most critical parameter for the 3 dB rejection bandwidth and thereby also the shape factor.

Changes in the cavity length turned out to be linear in center frequency f_0, 3 dB rejection bandwidth and shape factor. The notch frequency shift of -11.32 GHz per mm is a sensitive response, but the dynamic range where to place the notch frequency is broad. Tuning the notch filter few GHz up or down is not considered to be a problem in terms of the passband coverage and 3 dB bandwidth. However, the notch depth can vary $\pm$10 dB due to the mechanical imperfections.

A way to improve the notch filter design is to enlarge the cavity diameter D exciting a third order TE_{01l} mode. This mode has the highest Q factor and thereby lowest conductor loss because there is no axial current component, i.e. $\mathbf{H}_\phi$=0. A disadvantage with the TE_{01l} mode is a limited passband coverage compared with the fundamental TE_{11l} mode, i.e. neighboring notches are much closer in frequency for higher order modes compared with the fundamental. However, a practical advantage of trying higher order modes is that the ratio D/pitch (of the tuning screw) becomes larger making adjustment mechanically more stable.

The temperature of the receiver box surroundings, where the notch filter is placed, is expected to be in the range between 22 and 35 °C. By a measurement setup with a convection heat source and a network analyzer it was found that the temperature drift at 25 °C is approximately -2.6 MHz/°C. This drift is limited and will downshift the resonance frequency of the notch filter by at most 33.8 MHz which is found acceptable. The most sensitive parts of the CTS receiver is the electronics, so using a temperature controlled chamber will minimize effects of temperature gradients.

ACKNOWLEDGMENTS

This work, supported by the European Communities under the contract of Association between EURATOM / Risø DTU, was partly carried out within the framework of the Eu-

ropean Fusion Development Agreement. The views and opinions expressed herein do not necessarily reflect those of the European Commission.

---

[1] N. C. Luhmann *et al.*, Fusion Sci. Tech., **53**, 335 (2008).

[2] D. H. Wagner *et al.*, Nucl. Fusion, **48**, 054006 (2008).

[3] D. H. Wagner *et al.*, IEEE Trans. Plasma Sci., **36**, 324 (2008).

[4] E. Westerhof *et al.*, Phys. Rev. Lett., **103**, 125001 (2009).

[5] F. Meo *et al*, Rev. Sci. Instrum., **79**, 0E501 (2008).

[6] F. Meo *et al.*, J. Phys.: Conf. Series, **227**, 012010 (2010).

[7] M. Salewski *et al.*, Nucl. Fusion, **50**, 035012 (2010).

[8] H. Bindslev *et al.*, Phys. Rev. Lett., **83**, 3206 (1999).

[9] S. K. Nielsen *et al.*, Phys. Rev. E, **77**, 016407 (2008).

[10] S. K. Nielsen *et al.*, in press at Plasma Phys. Control. Fusion (2010).

[11] R. Behn *et al.*, Phys. Rev. Lett., **62**, 2833 (1989).

[12] S. B. Korsholm *et al.*, submitted (2010).

[13] M. Stejner *et al.*, in press at Rev. Sci. Instrum., Proceedings 18th Topical Conference on High Temperature Plasma Diagnostics (2010).

[14] S. B. Korsholm *et al.*, Nucl. Instrum. and Methods in Phys. Res., Proceedings of 1st International Conference on Frontiers in Diagnostic Technologies (2010).

[15] V. Furtula *et al.*, in press at Rev. Sci. Instrum, Proceedings 18th Topical Conference on High Temperature Plasma Diagnostics (2010).

[16] M. Salewski *et al.*, Rev. Sci. Instrum., **79**, 10E729 (2008).

[17] B. Piosczyk *et al.*, Fusion Engineering and Design, **66-68**, 481 (2003).

[18] A. Kasugai *et al.*, Nuclear Fusion, **48**, 054009 (2008).

[19] E. M. Choi *et al.*, J. Phys.: Conf. Series, **25**, 1 (2005).

[20] K. Felch *et al.*, J. Phys.: Conf. Series, **25**, 13 (2005).

[21] S. B. Korsholm *et al.*, Burning Plasma Diagnostics, **988**, 118 (2008).

[22] F. Leipold *et al.*, Rev. Sci. Instrum., **80**, 093501 (2009).

[23] M. Salewski *et al.*, Plasma Phys. Control. Fusion, **51**, 035006 (2009).

[24] M. Salewski *et al.*, Nucl. Fusion, **49**, 025006 (2009).

[25] G. Vayakis *et al.*, Nuclear Fusion, **46**, S836 (2006).

[26] G. Perez *et al.*, Fusion Engineering and Design, **84**, 1488 (2009).

[27] G. Vayakis *et al.*, Fusion Engineering and Design, **53**, 221 (2001).

[28] E. de la Luna JET-EFDA contributors (AIP, 2008) pp. 63–72.

[29] P. Woskov, Proceedings of LAPD-13 (2007).

[30] Y. Dryagin *et al.*, Int. J. Infrared Millimeter Waves, **17**, 1199 (1996).

[31] T. Geist and M. Bergbauer, Int. J. Infrared mm Waves, **15**, 2043 (1994).

[32] G. G. Denisov *et al.*, in *33rd International Conference on Infrared, Millimeter and Terahertz Waves, 2008. IRMMW-THz 2008* (2008) pp. 1–2.

[33] A. Krämer-Flecken *et at.*, Fusion Eng. Des., **56-57**, 639 (2001).

[34] G. G. Denisov *et al.*, Int. J. Infrared Millimeter Waves, **16**, 1231 (1995).

[35] D. A. Lukovnikov *et al.*, in *3rd International Conference on Infrared, Millimeter and Terahertz Waves, 2002. IRMMW-THz 2002* (2002) pp. 1029–1032.

[36] P. Goldsmith and H. Schlossberg, IEEE Transactions on Microwave Theory and Techniques, **28**, 1136 (1980).

[37] G. G. Denisov *et al.*, in *Proc. 18th Int. Conf. Infrared and Millimeter Waves, 353* (1993) p. 353.

[38] Z. Shen *et al.*, Plasma and Fusion Research: Regular Articles, **2**, 1 (2007).

[39] P. Woskoboinikow, W. Mulligan, and R. Erickson, IEEE Journal of Quantum Electronics, **19**, 4 (1983).

[40] G.Matthaei, L.Young, and E.M.T.Jones, *Microwave Filters, Impedance-Matching Networks, and Coupling Structures* (Artech House, 685 Canton Street, Norwood, MA 02062, 1980).

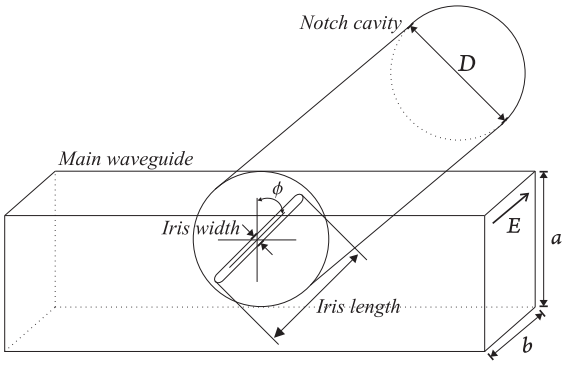

FIG. 1. T-junction aperture coupling using iris and horizontal cavity scheme.

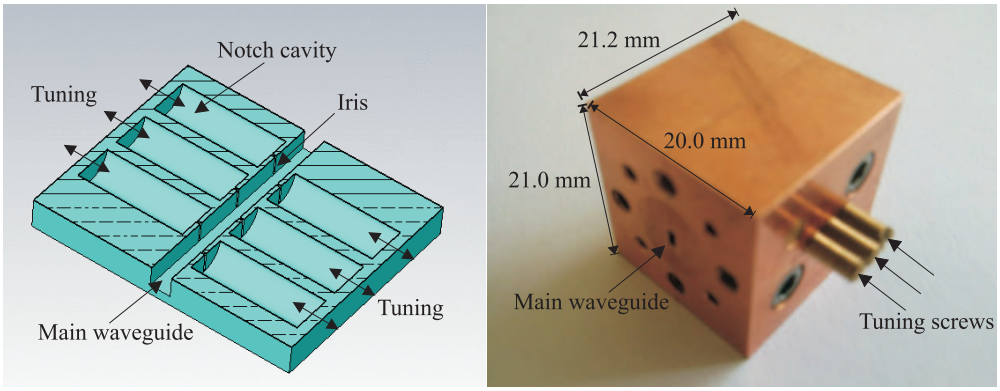

FIG. 2. Left: planar cut of the notch filter. Right: the constructed notch filter with tuning screws. The adjustment screws are not depicted in the sketch.

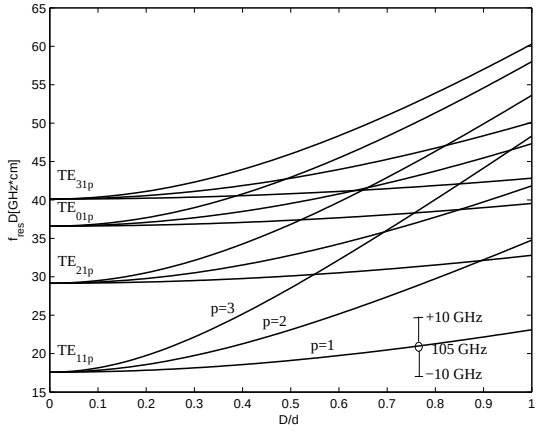

FIG. 3. TE mode chart for the first four modes using a cylindrical cavity resonator. The mode characteristics become straight lines if one plots $[f_r D]^2$ versus $[D/d]^2$. The circle shows the point of resonance in our design.

	Main waveguide	Resonator Cavity
Mode	TE_{011}	TE_{111}
Vacuum λ_0 [mm]	2.86	2.86
Cut-off λ_c [mm]	4.06	3.41
Waveguide λ_g [mm]	4	5.2

TABLE I. Characteristic λ values for the main rectangular waveguide and the cylindrical resonator waveguide.

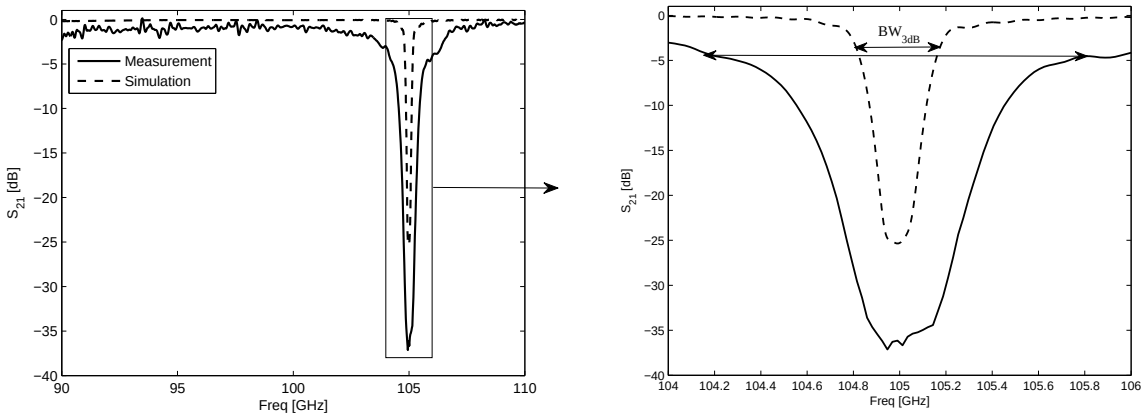

FIG. 4. A wide band and a narrow frequency band with a zoom close to the notch. The two lines on the right figure show 3 dB bandwidth, BW_{3dB} with respect to carrier, for the simulated and constructed notch filter.

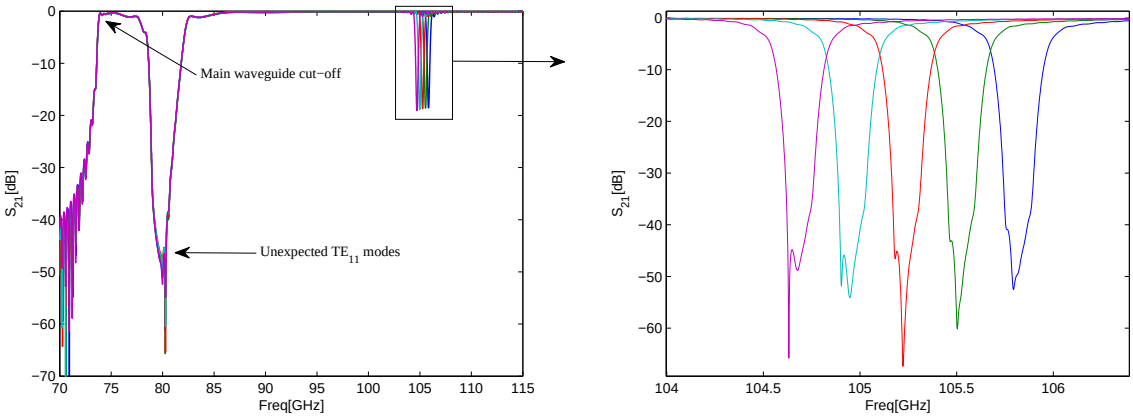

FIG. 5. S-parameter narrowband simulation showing 5 different cavity lengths.

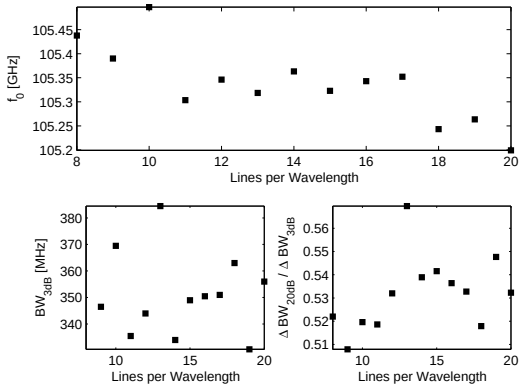

FIG. 6. Center frequency (upper), 3 dB bandwidth (lower-left), and shape factor (lower-right) are plotted versus lines per wavelength (L/λ_0).

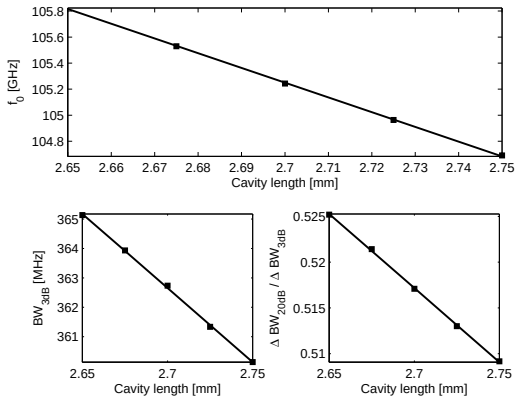

FIG. 7. Sensitivity of the center frequency f_0, the 3 dB bandwidth, and the shape factor to changes in the *cavity length*, see fig. 1. Symbols: simulations; line: least squares fit.

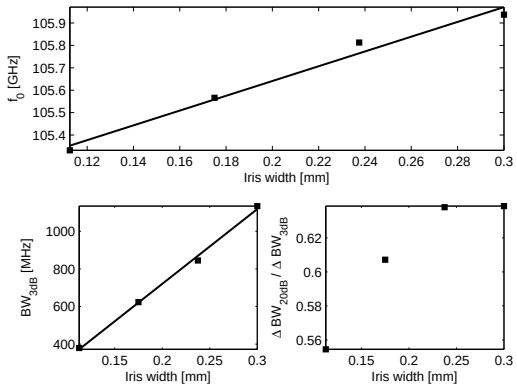

FIG. 8. Sensitivity of the center frequency f_0, the 3 dB rejection bandwidth, and the shape factor to changes in the *iris width*.

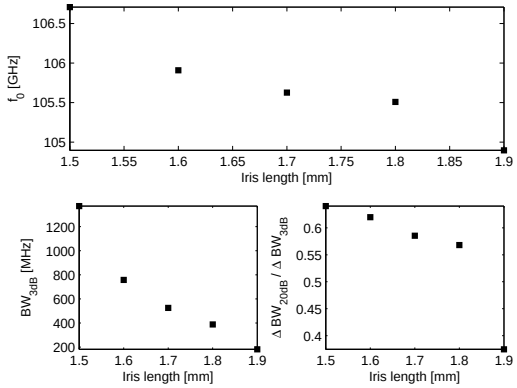

FIG. 9. Sensitivity of the center frequency f_0, the 3 dB bandwidth, and the shape factor to changes in the *iris length*. Symbols: simulations; line: least squares fit.

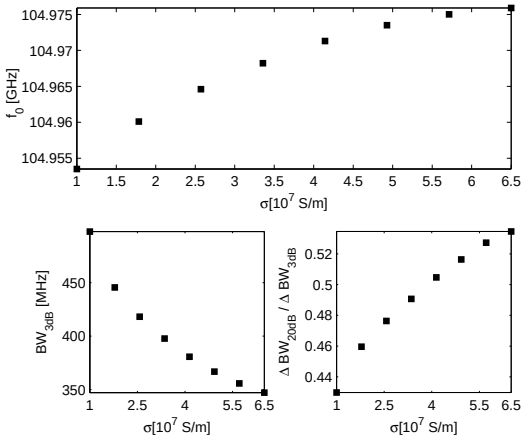

FIG. 10. Center frequency (upper), 3 dB bandwidth (lower-left), and shape factor (lower-right) are plotted versus conductivity corresponding to good conductors.

	Center freq. [GHz/mm]	3 dB bandwidth [GHz/mm]	Shape factor [mm^{-1}]
Cavity length	**-11.32**	**-0.05**	**-0.16**
Iris length	-8.0	-6.13	-1.93
Iris width	**3.3**	**3.98**	0.84

TABLE II. Sensitivity analysis investigation: impact on key characterization parameters by varying the design lengths (filter geometry). The bold numbers are slopes fitted using least squares method while the others are determined by the largest absolute gradient in the simulation range.